Available online at www.sciencedirect.com

ScienceDirect

journal homepage: www.elsevier.com/locate/he

Catalytic activity of Co–Ag nanoalloys to dissociate molecular hydrogen. New insights on the chemical environment

Guillermo Ortega, Estefanía Germán, María J. López, Julio A. Alonso*

Departamento de Física Teórica, Atómica y Optica, University of Valladolid, 47011 Valladolid, Spain

HIGHLIGHTS

- Alloying Co clusters with Ag improves their catalytic activity towards hydrogen.
- Hydrogen adsorbs preferentially on the Co atoms of the CoAg nanoalloys.
- Adsorption sites are determined by host coordination and chemical environment.
- Activation barriers for H_2 dissociation on CoAg nanoalloys are small.

ARTICLE INFO

Article history:
Received 22 February 2022
Received in revised form
9 April 2022
Accepted 10 April 2022
Available online 6 May 2022

Keywords:
Nanoalloys
Co–Ag clusters
Hydrogen adsorption
Heterogeneous catalysis

ABSTRACT

Adsorption of molecular hydrogen on the surface of catalytic metal nanoparticles and its dissociation in atomic hydrogen are processes of interest in many chemical technologies. As in other chemical reactions, alloying can improve the efficiency of the catalysts. By focusing on Co_6, Co_5Ag, Co_3Ag_3 and $CoAg_5$, we explore the effect of changing the relative concentration of the two components in small Co_mAg_n clusters, a peculiar nanoalloy because Co and Ag do not form bulk solid alloys. Molecular hydrogen adsorbs preferentially on the Co atoms, and the binding is mainly due to the electrical polarization of the charges of adsorbate and host. The preference for Co sites and the trend in the strength of the H_2-cluster binding are explained by the combination of two effects characterizing the host environment. One of these is geometric, arising from the degree of exposure of the host atom: the lower the atomic coordination of the host atom, the stronger its bonding with H_2. The second effect, newly identified, reveals the importance of the chemical nature of the host atom environment: host Co atoms having both Co and Ag neighbors maintain their capacity to bind hydrogen more intact than those with only Co neighbors. The alloy nanoclusters catalyze the dissociation of adsorbed H_2 by building up quite small activation barriers. After dissociation, the H atoms occupy bridge positions between Co atoms (between Co and Ag in $CoAg_5$). H_2 adsorption and dissociation may trigger structural transformations of the cluster. The work shows that the adsorption and dissociation properties of H_2 can be tuned by varying the relative composition of the two atomic species in the nanoalloy.

* Corresponding author.
E-mail address: maria.lopez@fta.uva.es (M.J. López).

https://doi.org/10.1016/j.ijhydene.2022.04.090

Introduction

The properties of metal clusters and nanoparticles make them candidates to build efficient and selective catalysts. First of all, the fraction of atoms on the cluster surface is substantial, and some of them are low coordinated at edges or corners, with the result that those atoms are quite active. On the other hand, the cluster properties are very sensitive to its size, in such a way that even the addition or removal of a single atom may change some cluster properties [1,2]. Haruta and coworkers noticed the extraordinary catalytic activity of small gold nanoparticles for some reactions [3,4], which is a remarkable feature because bulk gold is a noble, unreactive metal. Following that first observation, clusters and nanoparticles of platinum [5–8], palladium [5,8–10], ruthenium [8], copper [5,11] silver [5,12,13], cobalt [5] and other transition metals [8] have been investigated, and it was found that these nanomaterials show prominent catalytic activity and high selectivity for different reactions.

Alloying provides a method to tune the properties of metallic clusters. In addition to cluster size, the relative concentration of the components introduces a variable that can be utilized to optimize the properties for specific applications. The best metal catalysts are scarce and expensive [14]. Alloying those metals with cheaper ones [15,16] would be desirable, and many cases are observed in which alloying improves the catalytic properties [17–23]. Another unexpected bonus is that nanoalloys can often be formed from metals which do not form bulk solid alloys. This effect has been studied in lead-aluminium [24–26], tin-aluminium [25,27], and cobalt-silver [28,29] clusters, and the reasons for the enhanced miscibility at the nanoscale have been elucidated. This effect increases the chances of finding efficient nanocatalysts.

A hydrogen economy based on the production of green hydrogen, the storage of hydrogen, and the conversion of hydrogen to electricity is nowadays viewed as an effective way to address the problems of an increasing global energy demand and the environmental pollution. In particular, hydrogen will be a critical factor in the transportation industry [30]. A process of interest in this and other technologies is the adsorption of molecular hydrogen on a substrate and its dissociation in atomic hydrogen. An energy of 4.52 eV is required to dissociate H_2 in the gas phase, but metal catalysts can lower substantially this value. Dissociation of H_2 on the surface of transition metals has been studied [31,32], and the relevance of low coordinated metal atoms at surface steps and at edges and corners of nanoparticles has been noticed [32–35]. Also interesting is the dissociation of H_2 on single-atom catalysts supported on oxide surfaces [36]. Dissociation of H_2 on the surface of metal clusters can induce the isomerization of the clusters, that is, a change of the cluster structure [37].

As said above, an important technological application is the use of hydrogen as a clean and non-contaminant fuel in cars, a process which is based on the fuel cell technology [38–40]. At present, hydrogen is stored on board of the vehicle in metallic cylinders as a gas compressed at high pressures, but porous and layered materials are being intensively investigated as candidates to store hydrogen [41–47]. The stored gas then feeds a fuel cell where H_2 is first dissociated in the anode, then passes through a proton-exchange membrane [40,48,49] and reacts with atmospheric oxygen. This process produces an electric current and releases only water vapor. The dissociation of H_2 in the anode of the fuel cell is catalyzed by metallic nanoparticles. Because platinum is too expensive, other materials have been explored [50]. In the context of hydrogen storage, the spillover mechanism [51–53] has been proposed as an explanation for the observed enhancement of hydrogen storage in porous carbons doped with metal atoms, clusters and nanoparticles [54–56]. In this process, incoming H_2 first dissociates on the surface of the metal nanoparticle, then the H atoms diffuse through the nanoparticle and spill over the carbon substrate. The process of hydrogen adsorption is also relevant in the operation of hydrogen sensors [57].

Adsorption and dissociation of H_2 on metallic nanoalloys has been explored by several groups, mainly by performing Density Functional calculations. Several of those works correspond to clusters of aluminium alloyed with other metallic elements. Molecular adsorption of H_2 on Na_3Al_5 and Na_5Al_5, studied by Tong et al. [58], leads to weak bonding on the two clusters. Dissociation of the molecule depends sensitively on the cluster size: is easy on Na_3Al_5, with activation barriers of 0.16–0.19 eV, but dissociation barriers on Na_5Al_5 are much higher. In Al clusters doped with a single Cr atom (Al_nCr (n = 1–13)), Guo found that H_2 preferently physisorbs on the Cr atom [59]. Dissociation is exothermic, with barriers which vary with cluster size (between 0.3 and 1.3 eV), and after dissociation the H atoms usually occupy positions on top of Al atoms or bridge positions between Al–Al pairs. Adsorption of H_2 on Al_6 and Al_5Ti was studied by Boruah and Kalita [60]. The presence of Ti enhances the binding energy of H_2 to the cluster in both the molecular and dissociated configurations, and also raises a barrier for dissociation which was not found in pure Al_6. In a combined experimental and theoretical investigation, the interaction of H_2 with rhodium doped aluminum clusters, $Al_nRh_2^+$ (n = 1–9), was investigated by Jia et al. [61], who used mass spectrometry, infrared spectroscopy, and density functional calculations. The thermodynamic preference for molecular versus dissociative adsorption of H_2 depends on the cluster size. In addition, substantial barriers against dissociation were predicted. These features explain the correlation observed between the measured abundances of the hydrogenated species and the calculated molecular adsorption energies. Clusters of magnesium containing transition metal impurities have also been investigated. Addition of H_2 to $Mg_{17}M$ clusters, where M indicates a 3d transition element, was investigated by Charkin and Maltsev [62]. The 3d impurity catalyzes the dissociation of H_2 and the barriers are quite small. Trivedi et al. studied adsorption and dissociation of H_2 on Mg_nCo clusters [63], and Mg_nRh clusters [64]. Adsorption of hydrogen on Ir–Pd clusters with 38 atoms and octahedral structure has been studied by Davis et al. [65] H_2 dissociates and chemisorbs more strongly on the Ir-rich clusters. From the experimental side, it has been found [66] that the hydrogen absorbing properties of carbon-supported Pd–Ni nanoalloys (two metals that are miscible in bulk) change with the Ni content of the nanoparticles. The presence of Ni hinders the formation of a hydride phase in the nanoalloys, and at an atomic concentration of 30% Ni the hydride phase does not form at ambient conditions.

In this work we investigate the interaction between hydrogen and nanoalloys of metal-pairs which do not form bulk solid alloys. For this purpose, we have selected cobalt-silver clusters. In a previous work [29], we performed density functional calculations to study the atomic and electronic structure, and the magnetic moments of Ag_mCo_n clusters with $m + n = 2–6$, 10, and 11, analyzing the reasons for the mixing between the two metals at the nanoscale. In this work we first investigate the interaction between molecular hydrogen and clusters with three selected compositions, Co_5Ag, Co_3Ag_3 and $CoAg_5$. H_2 adsorption induces changes in the structure of Co_3Ag_3 and $CoAg_5$. An analysis of the trend displayed by the H_2 adsorption energies reveals the importance of both the geometric environment around the host metal atom (characterized by the number of neighbors) and the chemical environment (characterized by the chemical nature of the neighbors). Dissociation of the adsorbed H_2 is studied next, and the activation barriers are predicted to be quite small in Co_5AgH_2 and $Co_3Ag_3H_2$, but dissociation is energetically unfavorable in $CoAg_5H_2$. Comparison of the results for the different Co_mAg_n clusters reveals that the relative concentration of the two atomic components provides a powerful tool to optimally tune the behavior of the clusters with respect to the adsorption and dissociation of hydrogen, a process involved in many catalytic processes.

Computational method

The electronic and atomic structures of the Co–Ag nanoalloys, bare and with hydrogen adsorbed, have been investigated using the spin-polarized Density Functional Theory (DFT) [67,68], implemented in the Quantum Espresso package of codes [69]. Only the external electrons are treated explicitly, and their interaction with core electrons has been modelled using the projected augmented wave (PAW) method [70,71]. An Ar core and 17 valence electrons were taken for Co, a Kr core and 11 valence electrons for Ag, and one valence electron for H. The calculations are based on a periodic supercell methodology, and a cubic cell of length 15 Å was employed. The large size of the cell guarantees a negligible interaction between images in neighboring cells. The one-electron wave functions are expanded on a basis of plane waves, and a cutoff energy of 50 Ry was used to ensure a strict convergence criterion in the calculations. The cutoff for the electronic density was 400 Ry. The Monkhorst-Pack scheme [72] was used to select a $2 \times 2 \times 1$ grid of k points in the first Brillouin zone. The generalized gradient approximation of Perdew-Burke-Ernzerhof (PBE) has been employed for the exchange-correlation functional [73], and dispersion was taken into account by Grimme's D3 method [74]. Previous experience indicates that this methodology works well in the study of the interaction between hydrogen and metallic clusters [75–77].

Bimetallic clusters Co_5Ag, Co_3Ag_3 and $CoAg_5$ have been investigated. The atomic structure of these clusters has been studied earlier [29], but we have fully re-optimized the structures performing a more extensive search. For this purpose, large sets of initial structures have been considered, taking into account not only different geometrical structures, but also permutational isomers [78,79]; that is, clusters with the same underlying structure but a different distribution of the Co and Ag atoms over the cluster sites. In the case of hydrogenated clusters, an extensive search of the structures of the bimetallic clusters with adsorbed molecular and dissociated H_2 has been performed by placing the molecule or the two H atoms in a large (although judicious) selection of the possible adsorption sites on all the identified structural and permutational isomers. In all cases, the initial structures have been fully optimized until the components of the forces acting on any of the cluster atoms are smaller than 0.05 eV/Å. The ground state structures of the free clusters sometimes change due to the presence of hydrogen.

Results and discussion

Structure and electronic properties of Co_5Ag, Co_3Ag_3 and $CoAg_5$

Previous experience indicates that the most common structures of Co_mAg_n clusters with a total of six atoms are planar, octahedral and incomplete pentagonal bipyramid (IPB) structures [29]. An IPB is a pentagonal bipyramid in which one of the atoms of the equatorial plane is missing. Focusing on those candidates (but not restricting the search of isomers to them, and considering all possible permutational isomers for each geometrical configuration) we have found the lowest energy structures plotted in Fig. 1. The cohesive energies per atom are given as insets. The cohesive energy per atom is defined in terms of the total energies of the cluster and the free atoms.

$$E_{coh}(Co_mAg_n) = [m\,E(Co) + n\,E(Ag) - E(Co_mAg_n)]/6 \quad (1)$$

The predicted lowest energy structure of Co_5Ag is three dimensional, an octahedron, like the structure of Co_6 found by Marín et al. [29]. But the Co_5Ag octahedron is a bit deformed because of the atomic size difference between Co (the small atom) and Ag (the large atom), which makes the Co–Ag larger than the Co–Co bond distances. Because of the deformation, the structure can be seen as a bipyramid in which the two heights are different. The structure of $CoAg_5$ is a pentagonal pyramid with the Co atom occupying the apex of the pyramid at a very small height of 0.17 Å above the basal plane, so the structure can be considered as quasi-planar. The first low lying isomer is planar, with a form close to an equilateral triangle (Ag_6 is an equilateral triangle [29]) and the Co atom in the middle of a triangle side. The small deformation that can be appreciated in Fig. 1 is again due to the difference between the interatomic Ag–Ag and Ag–Co distances. The lowest energy structure found for Co_3Ag_3 is a slightly deformed planar triangle. The Ag atoms form the vertices of the triangle, and the Co atoms are in the middle of the triangle sides. The three Co atoms form a central core surrounded by the Ag atoms. The cohesive energy of Co_3Ag_3 is 1.99 eV/atom, and the spin magnetic moment is $\mu(Co_3Ag_3) = 6\ \mu_B$. A low-lying isomer with (deformed) octahedral structure exists, with the Ag and Co atoms segregated in different parts of the cluster. Its cohesive

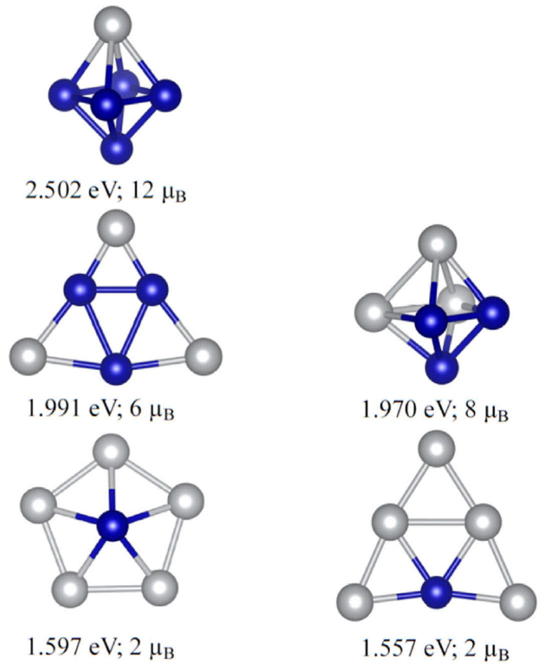

Fig. 1 – Calculated lowest energy structures of Co_5Ag, Co_3Ag_3, and $CoAg_5$, on the left panels, and some selected low-lying isomers on the right panels. The cohesive energy per atom (in eV) and the total magnetic moment (in Bohr magnetons) are given for each cluster. Blue and grey spheres represent Co and Ag atoms, respectively. (For interpretation of the references to color in this figure legend, the reader is referred to the Web version of this article.)

energy is 1.97 eV/atom, and the magnetic moment is $\mu = 8\ \mu_B$. Co_3Ag_3 is in the middle of the Co_mAg_n family with $m + n = 6$. The structure of the clusters on the Co-rich side of this family is octahedral, and it is planar or quasi-planar on the Ag-rich side [29]. The two trends enter in conflict in Co_3Ag_3, in which case the octahedral and planar structures are close in energy. The cohesive energy per atom increases as the proportion of Co atoms in the cluster increases, because the Co–Co bonds are significantly stronger than Ag–Ag and Co–Ag bonds. As expected, the magnetic moment of the cluster increases with the proportion of Co atoms. The ground state structures of Co_3Ag_3 and $CoAg_5$ found here are different, and more stable, than those reported previously [29].

Adsorption of molecular hydrogen

To study molecular adsorption, an H_2 molecule was initially placed on the host cluster on many different adsorption positions and orientations, and the structures were reoptimized. The calculations reveal that adsorption of the molecule on top of host Co atoms is energetically preferred compared to: 1) adsorption on top of Ag atoms, 2) adsorption on bridge sites (Co–Co, Ag–Ag and Co–Ag), 3) adsorption on hollow triangular sites. This result agrees with previous work on pure Co clusters [80]. The most stable adsorption configurations are shown in Fig. 2, and the corresponding adsorption energies are given in Table 1. The adsorption energy of H_2 is defined in terms of the energies of the reactants and final product, as

$$E_{ads}(H_2 \text{ on } Co_mAg_n) = E(H_2) + E(Co_mAg_n) - E(Co_mAg_nH_2). \quad (2)$$

Here, $E(Co_mAg_n)$ is the energy of the bare cluster in its lowest energy configuration. Fig. 2 shows that Co_5Ag maintains its structure after adsorption of H_2, and the adsorption energy is 0.426 eV. It can be noticed that the H_2 molecule is attached in Co_5Ag to a Co atom of the equatorial plane, and not to the Co atom in the apex, and this will be discussed later. On the other hand, the structures of Co_3Ag_3 and $CoAg_5$ change after adsorption of H_2. The new structure of Co_3Ag_3 is three-dimensional: a pyramid, with an Ag atom attached on an edge of the base of the pyramid. The H_2 molecule is on top of the Co atom at the pyramid apex. The adsorption energy of H_2 on Co_3Ag_3 is 0.653 eV. The new structure of $CoAg_5$ can be seen as a deformed IPB: one of the Ag atoms of the original pentagonal pyramid moves out of the basal plane, giving rise to an incomplete pentagon with a Co atom above and an Ag atom below the equatorial plane. The adsorption energy of H_2 on $CoAg_5$ is 0.647 eV.

An interesting feature is the lower adsorption energy of H_2 on Co_5Ag as compared to the other two clusters. The atomic coordination numbers CN of the host atoms in metal surfaces and nanoparticles are known to be inversely correlated with the adsorption energies of small molecules on those atoms: the lower CN of the host atom, the stronger the adsorption energy [81]. In other words, more exposed host atoms are more reactive. The number of metal atom neighbors of the host Co atom in the three clusters of Fig. 2 is 4, 4, and 5 for Co_5AgH_2, $Co_3Ag_3H_2$, and $CoAg_5H_2$, respectively, and these numbers do not show a correlation with the H_2 adsorption energies. But one can appeal to the generalized coordination numbers CN_g introduced by Calle-Vallejo et al. [33]. In order to assign CN_g to an atom i with n_i nearest neighbors, those neighbors are counted and weighted by their own usual coordination numbers CN. That is,

$$CN_g(i) = \sum_{j=1}^{n_i} \frac{CN(j)}{CN_{max}} \quad (3)$$

where j runs over the n_i nearest neighbors of atom i, and CN_{max} is a normalizing factor that we take as $CN_{max} = 5$, the maximum coordination number observed in these clusters. In Co_5AgH_2, the host Co atom has $CN = 4$, and each one of the nearest neighbors also has $CN = 4$; so CN_g(host Co) = 3.2. On the other hand, in $Co_3Ag_3H_2$ the host Co atom has $CN = 4$, and two of those neighbors have $CN = 4$, while the other two neighbors have $CN = 3$, leading to CN_g(host Co) = 2.8. In $CoAg_5H_2$, the host Co atom has $CN = 5$, and all those neighbors have $CN = 3$, so CN_g(host Co) = 3. This means that the highest CN_g occurs in Co_5AgH_2, and the lowest occurs for the intermediate composition $Co_3Ag_3H_2$, in agreement with the trend shown by the H_2 adsorption energies. One should notice, however, that the H_2 adsorption energy of $CoAg_5H_2$ is only 0.006 eV lower than that of $Co_3Ag_3H_2$, despite the CN_g value of the former being higher than that of the later. This indicates that additional factors affect the adsorption of hydrogen, as it is explained below.

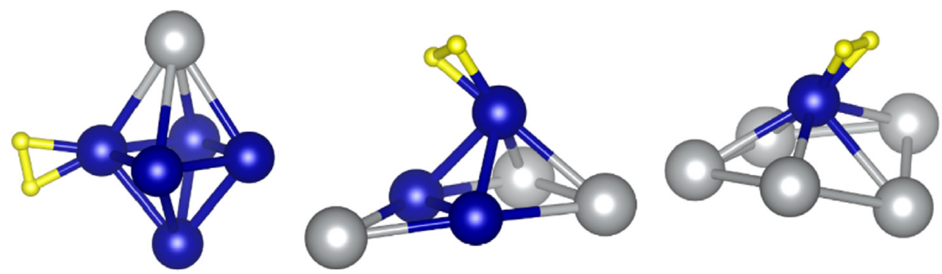

Fig. 2 – Calculated lowest energy structures for H_2 adsorbed on Co_5Ag, Co_3Ag_3, and $CoAg_5$. Blue, grey and yellow spheres represent Co, Ag and H atoms, respectively. (For interpretation of the references to color in this figure legend, the reader is referred to the Web version of this article.)

The redistribution of the electron density $\Delta\rho(\vec{r})$ which occurs when H_2 is adsorbed, defined

$$\Delta\rho(\vec{r}) = \rho_{Co_mAg_nH_2}(\vec{r}) - \rho_{H_2}(\vec{r}) - \rho_{Co_mAg_n}(\vec{r}) \quad (4)$$

is plotted in Fig. 3 for the three clusters. The densities of the Co_mAg_n and H_2 subsystems required in eq. (4) are obtained by calculations for those isolated subsystems with the structure they have in the combined system. Finally, the density of electronic states, DOS, of the three clusters is plotted in Fig. 4. The energy zero corresponds to the Fermi energy, and the upper and lower panels in each Figure stand for electronic states with up and down spin orientations, respectively.

An important observation in the DOS of the three systems is that the states associated with the adsorbed H_2 (one spin up state and one spin down state) are well separated from the cluster states and their binding energies are about 8 eV. This indicates that there is no hybridization between H_2 states and cluster states, and that the source of the bonding of H_2 to these clusters is mainly the polarization of the electronic charge of the molecule and the metal atoms and the electrostatic interaction between those polarized charge distributions. The dispersion interactions, given in Table 1, make a relatively minor contribution. The charge polarization can be appreciated in the electron density redistributions of Fig. 3. The charge polarization affects the H_2 molecule and Co atoms, especially the Co atom hosting the H_2 molecule, and to a lesser extent the other Co atoms, but does not affect the Ag atoms. We interpret this as revealing that the charge of the Ag atoms of the nanoalloy is less polarizable than the charge of the Co atoms, and we propose this to be the reason for the preferential H_2 adsorption on Co atoms seen in Fig. 2. This is confirmed by the DOS plots of Fig. 4. The states close to the Fermi energy are the main contributors to the charge polarization, and these states have Co character in Co_5Ag and Co_3Ag_3, and Co character with some contribution of Ag character in $CoAg_5$. In fact, the shapes of the highest occupied molecular orbital (HOMO) and lowest unoccupied molecular orbital (LUMO) of bare Co_5Ag, shown in Fig. 5, clearly display Co character, and those of bare $CoAg_5$ display mixed character. The atomic charges in the $Co_mAg_nH_2$ complexes, calculated by the Bader method [82–84], are given in Table 2. The absolute values of those charges are very small, in general below 0.10 eV, confirming the interpretation of the bonding

Table 1 – Adsorption energies of molecular and dissociated H_2. Values of $E_{ads}(H_2)$ in brackets give the dispersion contribution. Also, magnetic moments of bare clusters and clusters with hydrogen.

	$\mu(Co_mAg_n)$ (μ_B)	$E_{ads}(H_2)$ (eV)	$\mu(Co_mAg_nH_2)$ (μ_B)	$E_{ads}(2H)$ (eV)	$\mu(Co_mAg_n2H)$ (μ_B)
Co_6 [80]	14	0.12	14	0.60	12
Co_5Ag	12	0.426 (0.064)	10	1.204	10
Co_3Ag_3	6	0.653 (0.149)	6	1.491	6
$CoAg_5$	2	0.647 (0.029)	2	0.479	2

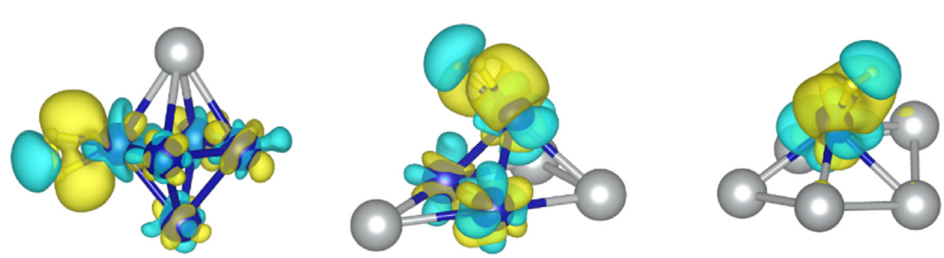

Fig. 3 – Density redistribution $\Delta\rho(\vec{r})$ for adsorption of H_2 on Co_5Ag, Co_3Ag_3, and $CoAg_5$. Yellow and blue colors mark surfaces of $\Delta\rho(\vec{r}) = +0.003\ e\text{Å}^{-3}$, and $-0.003\ e\text{Å}^{-3}$, respectively. That is, the electron density increases (decreases) in the yellow (blue) regions. (For interpretation of the references to color in this figure legend, the reader is referred to the Web version of this article.)

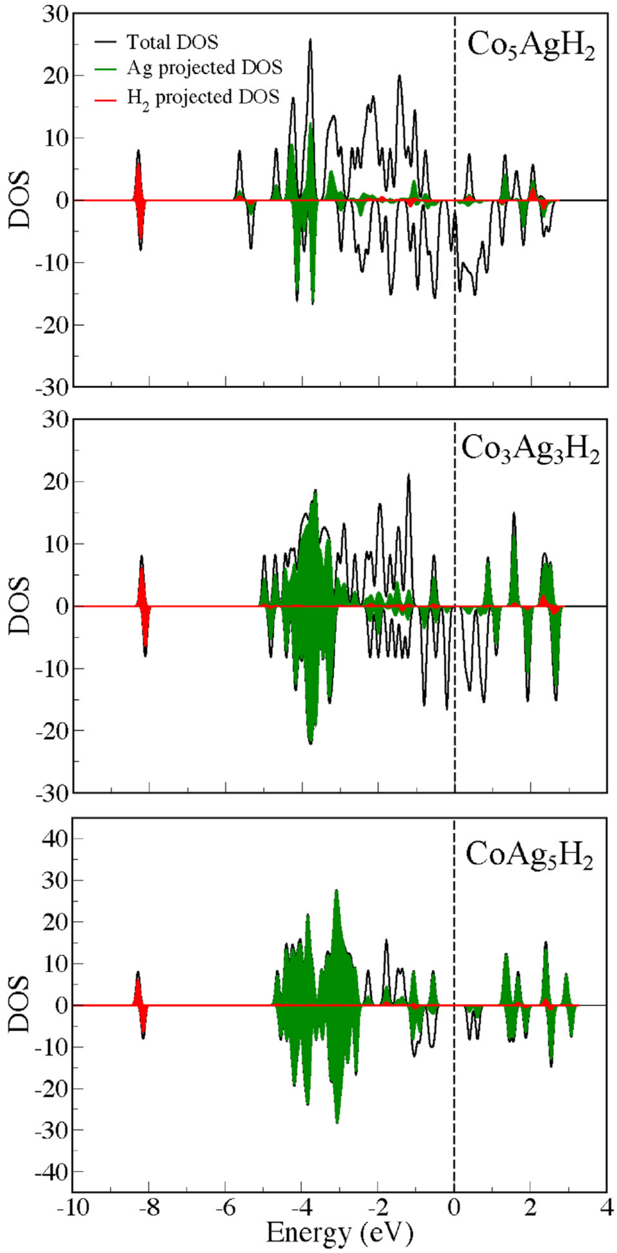

Fig. 4 – Electronic density of states (DOS) of Co_5AgH_2, $Co_3Ag_3H_2$, and $CoAg_5H_2$. The zero energy represents the Fermi energy. The DOS is separated in spin up (upper panel) and spin down (lower panel) components. DOS projected on the Ag atoms are marked in green color. The two states associated to the H_2 molecule, colored in red, are well separated from the rest. (For interpretation of the references to color in this figure legend, the reader is referred to the Web version of this article.)

between H_2 and the cluster given above. The only case in which a sizable charge is noticed corresponds to the Co atom in $CoAg_5$, and the charge lost by the Co atom is redistributed between all the other atoms in the complex.

The transition from the planar to a three dimensional structure of Co_3Ag_3 upon adsorption of H_2 is an interesting feature. Bare Co_3Ag_3 is planar, with the Co atoms located in the middle of the edges of the triangular structure (see Fig. 1). Those are less exposed than the vertex sites. Then, if we focus on one of the Ag–Co–Ag sides of the original triangle, the strategy adopted by the cluster is lifting the Co atom up from the plane and approaching the positions of those two Ag atoms until an Ag–Ag bond is formed. These rearrangements lead to the emergence of the pyramid seen in Fig. 2, and the lifted up Co atom now occupies an exposed vertex site. There is an energetic cost in transforming the structure of the cluster, small here because Co_3Ag_3 is in the borderline between two and three-dimensional structures, but this cost is more than compensated by the enhanced strength of the H_2–Co interaction. In fact, the structural transformation occurs spontaneously; that is, without activation barrier, as soon as the H_2 molecule is attached to one of the Co atoms of Co_3Ag_3. In spite of the energy toll paid by the structural change, the adsorption binding energy of H_2 on Co_3Ag_3 is higher than the adsorption energies on Co_5Ag and $CoAg_5$. We have discussed above that this is due to a combination of geometrical and polarization charge effects, and we now go one step further in this argument. The adsorption energy of H_2 on Co_5Ag (0.426 eV) is smaller than on Co_3Ag_3 (0.653 eV) and $CoAg_5$ (0.647 eV), because in Co_5Ag the host Co atom is more tightly bound in the cluster. It is linked to three Co atoms, forming strong bonds with them, and to one Ag atom, forming a weaker bond. On the other hand, the host Co atom in Co_3Ag_3 is linked to two Co atoms and two Ag atoms. That is, the chemical environment keeps the host Co atom more tightly bound in Co_5Ag as compared to Co_3Ag_3, and consequently the host Co atom in Co_5Ag is less polarizable. Confirmation is obtained by comparing these results with the adsorption energy of H_2 on pure Co_6, which is even lower, 0.129 eV [80]. The structure of Co_6 in Co_6H_2 is an octahedron so the coordination numbers of the host Co atom are $CN = 4$, and $CN_g = 3.2$, just as in Co_5AgH_2, and one could expect a similar adsorption energy. However, the host Co atom is bonded to four Co atoms in Co_6, and is thus more tightly bound than in Co_5AgH_2, and then the environment of the adsorbed H_2 molecule is less polarizable. As shown above, the adsorption energy of H_2 on $CoAg_5H_2$ is smaller than on $Co_3Ag_3H_2$, a result which is consistent with the argument based on the generalized coordination numbers. However, based on the CN_g values of the host Co atoms, 3 and 2.8 respectively, one perhaps could expect a smaller value of the adsorption energy of H_2 on $CoAg_5H_2$. The explanation is again the nature of the chemical environment. The Co atom in $CoAg_5H_2$ has an environment formed by Ag atoms exclusively, and the weak Co–Ag bonds make the environment of the adsorbed H_2 molecule more polarizable.

In summary, by considering the sequence Co_6, Co_5Ag, Co_3Ag_3, $CoAg_5$, the trend in the reactivity towards H_2, measured by the adsorption energy, can be explained by a combination of two ingredients. One is the generalized coordination number of the host Co atom, which accounts for the geometrical nature of the environment. This would be sufficient in pure metal clusters and nanoparticles. However, in alloy clusters it is useful to consider an additional factor, the chemical nature of the environment, motivated by the presence of two different atomic species in the cluster. Appeal to the chemical environment also explains why H_2 prefers binding to an equatorial Co atom of Co_5AgH_2 and not to the

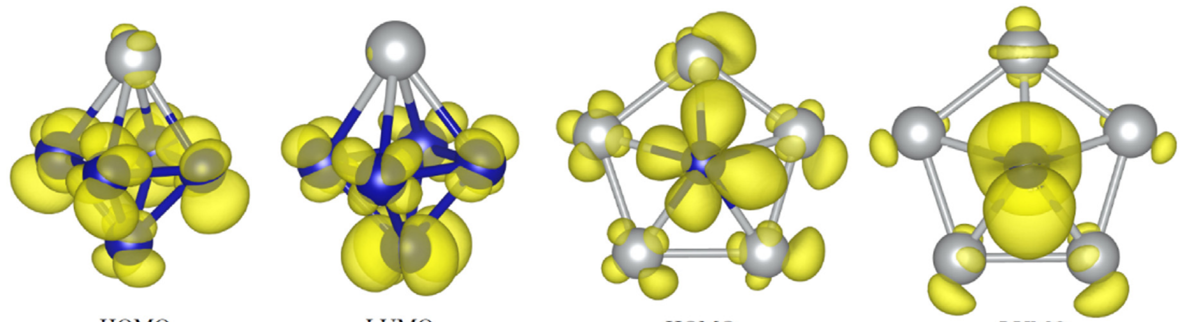

Fig. 5 – Spatial distribution of the electron density corresponding to the HOMO (left) and LUMO (right) orbitals of bare Co_5Ag and $CoAg_5$. The value of the electron density in the isodensity surfaces shown in yellow is 0.0008 $e\text{Å}^{-3}$. (For interpretation of the references to color in this figure legend, the reader is referred to the Web version of this article.)

Table 2 – Bader atomic charges. Negative (positive) values indicate a net excess (defect) of electrons in the atom. The ordering of the atoms in each individual column is arbitrary. Charges in bold face correspond to metal atoms in direct contact with the H_2 molecule or the H atoms.

	Co_5Ag-H_2	Co_5Ag-2H		$Co_3Ag_3-H_2$	Co_3Ag_3-2H		$CoAg_5-H_2$	$CoAg_5-2H$
Co	0.08	−0.01	Co	**0**	**0.39**	Co	**0.40**	**0.38**
Co	0	**0.20**	Co	−0.01	**0.09**	Ag	−0.07	**0.07**
Co	0	**0.21**	Co	0.06	**0.09**	Ag	−0.05	−0.02
Co	−0.04	**0.20**	Ag	0	0.01	Ag	−0.07	−0.04
Co	**0.07**	−0.01	Ag	0.02	0.05	Ag	−0.07	−0.09
Ag	−0.01	0.01	Ag	0.01	0.02	Ag	−0.07	**0.05**
H	−0.01	−0.30	H	0	−0.33	H	−0.03	−0.16
H	−0.03	−0.30	H	−0.09	−0.32	H	−0.05	−0.19

apex Co atom. The generalized coordination numbers of both host Co atoms are the same, but the chemical environment of the equatorial Co atom is more favorable because one of the neighbors is a Ag atom. The conclusion is that the alloy concentrations Co_3Ag_3 and $CoAg_5$ are more favorable for adsorption of molecular hydrogen than the Co reach concentrations Co_5Ag and Co_6 because of the cooperation of those two factors.

Dissociative adsorption of hydrogen

The behavior of the $Co_mAg_nH_2$ clusters upon dissociation of the H_2 molecule is complex. The dissociation of H_2 on Pd_6 supported on a graphene vacancy is accompanied by a structural transformation of the metal cluster [37], and one can also expect structural transformations in the Co_mAg_n clusters. The calculated lowest-energy dissociated configurations are given in Fig. 6. If one starts with the molecular adsorption structures of Fig. 2, the dissociation of H_2 induces structural transformations in Co_3Ag_3 and $CoAg_5$. The adsorption energies are given in Table 1. In this case the adsorption energy is defined

$$E_{dissoc\text{-}ads}(Co_mAg_n2H) = E(H_2) + E(Co_mAg_n) - E(Co_mAg_n2H) \quad (5)$$

where $E(Co_mAg_n2H)$ is the global minimum energy of the system formed by the dissociatively adsorbed molecule, that is, two H atoms on Co_mAg_n, and $E(Co_mAg_n)$ is the global minimum energy of the bare cluster, that is, with the structure shown in Fig. 1.

At difference with molecular adsorption, the H atoms now form bridges between Co atoms, or between the Co atom and Ag atoms in $CoAg_5$. The bridge positions optimize the chemical bonding. This can be seen by analyzing the redistribution of the electron density $\Delta\rho(\vec{r})$,

$$\Delta\rho(\vec{r}) = \rho_{Co_mAg_n2H}(\vec{r}) - \rho_{2H}(\vec{r}) - \rho_{Co_mAg_n}(\vec{r}) \quad (6)$$

plotted in Fig. 7 for the three clusters. In this equation, the density of Co_mAg_n corresponds to a calculation for the bare alloy cluster with precisely the same structure it has in Co_mAg_n2H, and $\rho_{2H}(\vec{r})$ represents the density of two free H atoms placed at the locations they have in Co_mAg_n2H. The three panels of Fig. 7 show accumulation of electronic charge in the regions occupied by the H atoms. Since the bonding involves electronic charge transfer, bridge positions between two atoms are more favorable than positions on top of one host atom. The most plausible explanation for the H atoms preferring bridge positions between Co atoms is that the electronegativity of Co in the Pauling scale is 1.8, while the electronegativity of Ag is 1.9. Then, electron transfer from Co atoms to the H atoms, with electronegativity 2.1, is easier. The atomic charges, calculated by the Bader method [82–84], are given in Table 2. Indeed, the H atoms carry an excess of about 0.2–0.3 electrons, and that charge is transferred mainly by the atoms forming bridges with H.

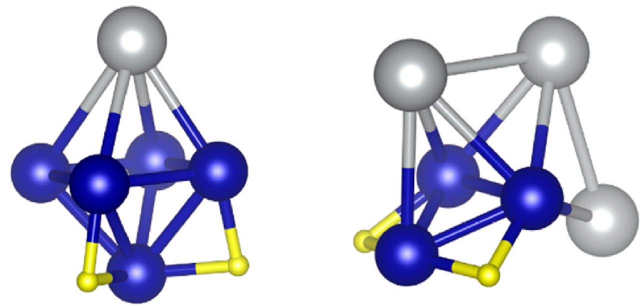

Fig. 6 – Calculated lowest energy structures for a dissociated hydrogen molecule on Co_5Ag, Co_3Ag_3, and $CoAg_5$. Blue, grey and yellow spheres represent Co, Ag and H atoms, respectively. (For interpretation of the references to color in this figure legend, the reader is referred to the Web version of this article.)

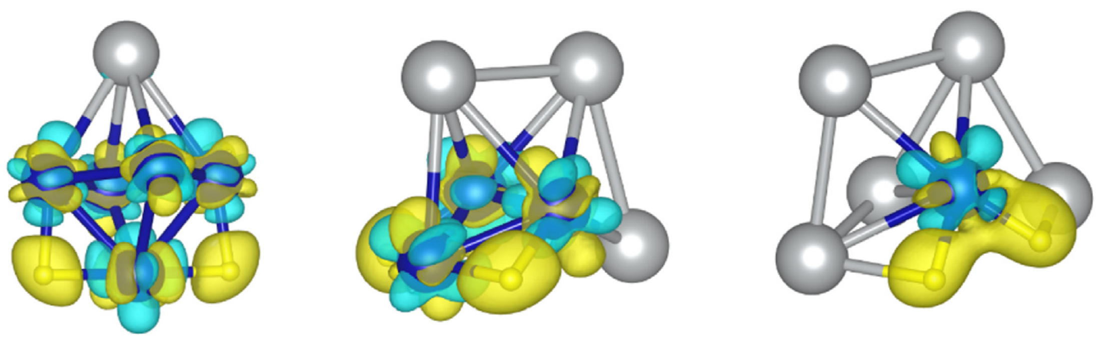

Fig. 7 – Electron energy redistribution $\Delta\rho(\vec{r})$ defined in eq. (6), associated to the dissociative adsorption of the hydrogen molecule on Co_5Ag, Co_3Ag_3, and $CoAg_5$. Yellow and light blue colors mark surfaces of constant $\Delta\rho(\vec{r}) = +0.008\ e\text{Å}^{-3}$, and $\Delta\rho(\vec{r}) = -0.008\ e\text{Å}^{-3}$, respectively. That is, the electron density increases (decreases) in the yellow (blue) regions. (For interpretation of the references to color in this figure legend, the reader is referred to the Web version of this article.)

The DOS plots in Fig. 8 show that the electronic states associated with the H atoms are again located in the region of high binding energies, but at difference with molecular adsorption those states have no pure H character. Instead, a strong hybridization between H and cluster states occurs.

The octahedral structure of Co_5Ag is preserved when the adsorbed H_2 molecule dissociates and the two H atoms form bridges between Co atoms of the equatorial plane of the octahedron and the Co atom in the apex. The dissociative adsorption energy, defined in eq. (5), is 1.204 eV. That definition of the dissociative adsorption energies allows to compare these with the molecular adsorption energies because the reference (H_2 and Co_mAg_n) is the same. The dissociative adsorption energy on Co_5Ag is larger than the molecular adsorption energy by a factor of three, in spite of the fact that dissociation of the free molecule is highly endothermic. This is due to the catalytic effect of the alloy cluster in lowering the dissociation barrier, and to the charge transfer and bonding discussed above. The dissociation barrier was calculated using the climbing image nudge elastic band (CI-NEB) method [85]. The dissociation path connecting the initial configuration of Co_5AgH_2 given in Fig. 2 and the final configuration of Co_5Ag2H given in Fig. 6 exhibits an activation barrier of only 0.031 eV. A few snapshots along the dissociation path are shown in Fig. 9. Dissociation occurs on top of the Co atom, and then the two H atoms move to bridge positions.

After dissociation of H_2 on Co_3Ag_3, a transformation of the structure of the cluster takes place. Its final structure is an IPB in which the two apex atoms are Co atoms. The H atoms are in bridge positions between the apex atoms and the Co atom of the equatorial plane. The dissociative adsorption energy on Co_3Ag_3 is 1.491 eV, larger compared to Co_5Ag in spite of the structural change. To explain this feature we can again appeal to the chemical environment. In Co_5Ag, the Co apex atom has four Co neighbors, and the Co atoms in the equatorial plane have three Co neighbors and one Ag neighbor. As noticed above, the Co–Co bonds are stronger than the Co–Ag bonds. On the other hand, in Co_3Ag_3 each of the Co atoms only has two Co neighbors (the rest of the neighbors are Ag atoms), so the bonding capacity of the Co atoms is less exhausted, and can form stronger bonds with the H atoms. This argument is supported by results for Co_6. In this cluster, all the Co atoms have four neighbors, and the dissociated adsorption energy, 0.60 eV, is lower [80]. The NEB dissociation path connecting the initial configuration of $Co_3Ag_3H_2$ given in Fig. 2 and the final configuration of Co_3Ag_32H given in Fig. 6 predicts a quite small activation barrier of 0.042 eV. A few snapshots along the dissociation path are shown in Fig. 10.

The structure of $CoAg_5H_2$ is intermediate between a pentagonal pyramid and an IPB (see Fig. 2), and dissociation of the hydrogen molecule drives the cluster structure to a nearly perfect IPB (see Fig. 6). The two H atoms form bridges between the Co atom and Ag atoms of the equatorial plane of the

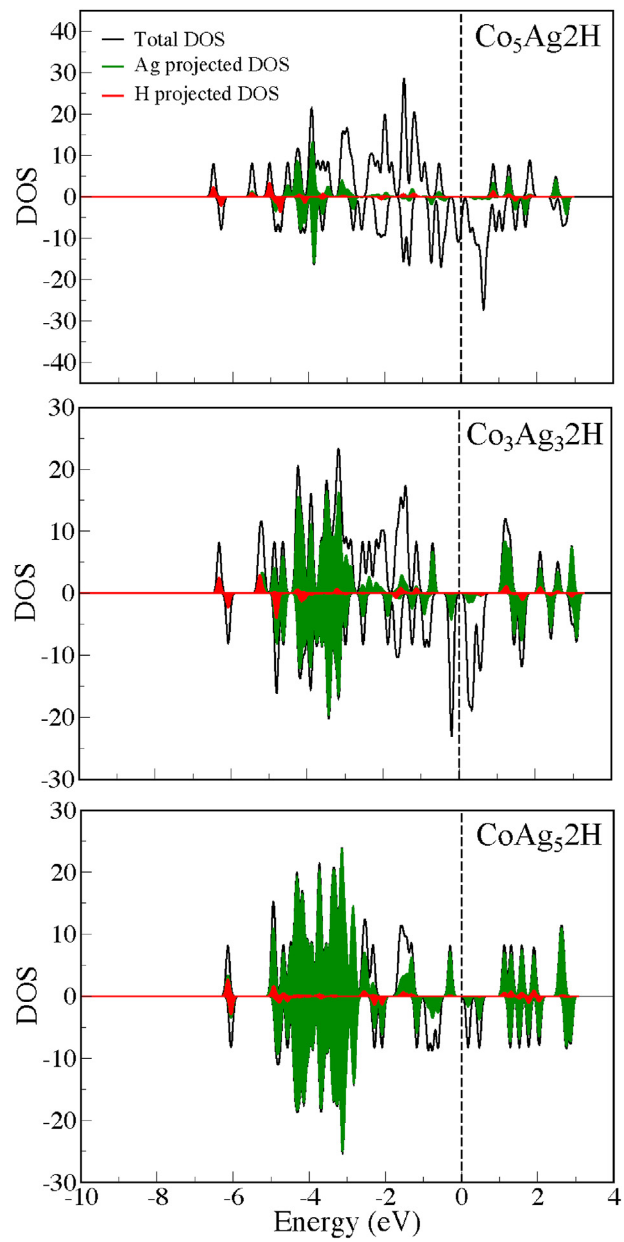

Fig. 8 – Electronic density of states (DOS) of Co_5Ag2H, Co_3Ag_32H, and $CoAg_52H$. The zero energy represents the Fermi energy. DOS is separated in spin up (upper panel) and spin down (lower panel) components. DOS projected on the Ag atoms is marked in green color. DOS projected on the H atoms is colored in red. (For interpretation of the references to color in this figure legend, the reader is referred to the Web version of this article.)

bipyramid. The dissociative adsorption energy is 0.479 eV, a lower value in comparison with Co_5Ag and Co_3Ag_3. Also, interestingly, the dissociative adsorption energy of H_2 on $CoAg_5$ is lower than the molecular adsorption energy (see Table 1); that is, dissociating the adsorbed molecule on $CoAg_5$ is an endothermic process. This is surprising, because usually the opposite occurs in metal and alloy nanoclusters [80,86–88]. The explanation of those features is that the energy cost of transforming the quasi-planar structure of $CoAg_5$ into a three-dimensional structure is

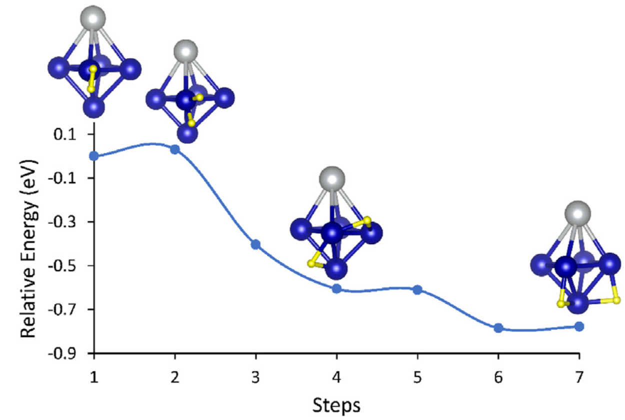

Fig. 9 – Energy curve and structural snapshots along the dissociation path of H_2 on Co_5Ag.

not compensated by the chemisorption energy of the two H atoms, because the bonding of H atoms to Ag atoms is weaker than the bonding to Co. A complementary view of this effect is that the electronic HOMO-LUMO gap of $CoAg_5H_2$ is substantial, 0.94 eV, and dissociation of H_2 lowers the gap to 0.47 eV, one half of the previous value. It is known that the magnitude of the electronic gap of a material correlates with its stability.

In summary, replacing Co atoms in Co_6 clusters with Ag results in most cases in an increase of the molecular and dissociative adsorption energy of H_2. The reason is that molecular adsorption occurs on top of Co atoms and dissociative adsorption occurs on bridge positions between Co atoms, and the bonding strength towards H and H_2 is higher when those Co atoms have some Ag neighbors, in comparison with the case of having only Co neighbors. Dissociation of the adsorbed H_2 takes place with small activation barriers. The composition rich in Ag, that is $CoAg_5$, represents an especial case, since H_2 dissociation is energetically unfavorable.

Evolution of the magnetic moments

The spin magnetic moments μ (taken as the difference between the number of electrons with spin up and spin down character in the spin density functional formalism) of the clusters, bare and

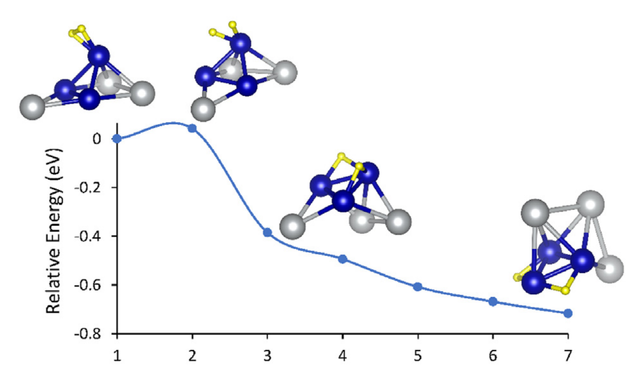

Fig. 10 – Energy curve and structural snapshots along the dissociation path of H_2 on Co_3Ag_3.

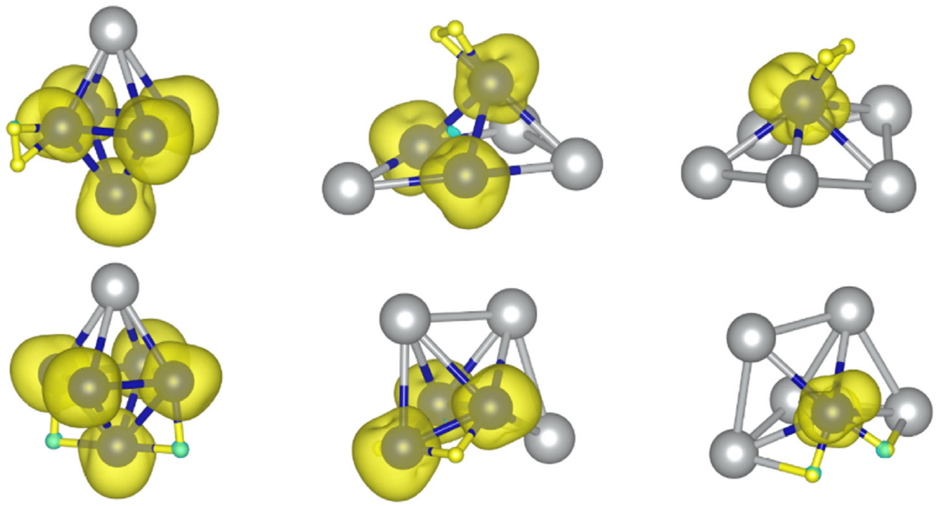

Fig. 11 – Spatial distribution of spin density in Co_5AgH_2, $Co_3Ag_3H_2$ and $CoAg_5H_2$ (upper panels), and Co_5Ag2H, Co_3Ag_32H and $CoAg_52H$ (lower panels). The spin isodensity surfaces plotted in yellow color correspond to $\Delta\rho_{spin}(\vec{r}) = +0.008$ e Å^{-3}. Minute regions in bright green color correspond to $\Delta\rho_{spin}(\vec{r}) = -0.008$ e Å^{-3}. (For interpretation of the references to color in this figure legend, the reader is referred to the Web version of this article.)

after molecular and dissociative adsorption of H_2 are compared in Table 1. The magnetic moments of the bare clusters show a strong dependence with the relative concentration of Co and Ag. This observation and the result $\mu(Cu_6) = 14\ \mu_B$ obtained by García-Díez et al. [80] indicate that the Co atoms are the main contributors to the cluster magnetism. This is confirmed by the DOS of Figs. 4 and 8. There is good matching between spin up and spin down DOS with Ag character, but an energy shift between spin up and spin down states with Co character is evident. The geometric structure can also influence the values of μ: the magnetic moments of the planar and three dimensional structures of Co_3Ag_3 shown in Fig. 1 amount to 6 μ_B and 8 μ_B, respectively. The presence of adsorbed hydrogen causes only a minor effect. It affects the magnetic moment of Co_6 and Co_5Ag, but not the magnetic moments of Co_3Ag_3 and $CoAg_5$.

Additional insight is obtained from the spatial distribution of the net spin density

$$\Delta\rho_{spin}(\vec{r}) = \rho\uparrow(\vec{r}) - \rho\downarrow(\vec{r}), \quad (7)$$

that is, the difference between the spin up $\rho_\uparrow(\vec{r})$ and spin down $\rho_\downarrow(\vec{r})$ components of the electron density at each point $\vec{r}$ in space. The integral of $\Delta\rho_{spin}(\vec{r})$ over the cluster volume gives the magnetic moment in units of μ_B. The spatial distributions of the spin magnetism in the Co_5AgH_2, Co_5Ag2H, $Co_3Ag_3H_2$, Co_3Ag_32H, $CoAg_5H_2$, and $CoAg_52H$ clusters are shown in Fig. 11. The net spin density is concentrated on the cluster regions occupied by the Co atoms, and the coupling is ferromagnetic.

Summary and conclusions

Metal nanoclusters find applications in catalysis, and the cluster size is a variable that can be tuned to optimize the catalytic performance. Alloying opens new prospects, because the relative concentration of the components introduces another variable that can be utilized to tailor the cluster properties. The best metal catalysts are scarce, and alloying with cheaper metals would be desirable if the properties are not degraded. Even more, nanoalloys can often be formed from metals which do not form bulk solid alloys. One of those cases is Co–Ag.

Adsorption and dissociation of H_2 is of interest in many catalytic processes. We have studied the adsorption of molecular hydrogen on the Co_5Ag, Co_3Ag_3 and $CoAg_5$ clusters using the density functional formalism, with the purpose of investigating the role played by the relative concentration of the Co and Ag. H_2 prefers to attach to Co atoms of those clusters, and the bonding is mainly electrostatic, due to the electric polarization of the charges of adsorbate and host. The adsorption sites and the strength of the bonding are explained by a combination of two factors reflecting the atomic environment of the host atom. One of those factors is geometric. The bonding between the molecule and the cluster is stronger when the atomic coordination of the host atom is lower; that is, when the host atom is well exposed [33,81]. The second effect reveals the importance of the chemical environment of the host atom. The bonding between Co atoms is stronger than the bonding between Co and Ag atoms. Thus, an environment formed by Co and Ag atoms preserves the bonding capacity of the host Co atom toward H_2 molecules more intact than an environment formed exclusively by Co atoms. A structural change occurs on Co_3Ag_3 and on $CoAg_5$ upon H_2 adsorption that can be interpreted as a cluster strategy to enhance the strength of the bonding with the adsorbate. Dissociation of the adsorbed H_2 molecule in two H atoms is easy because the activation barriers are quite low. The H atoms occupy bridge positions between Co atoms (Co and Ag in $CoAg_5$). H_2 dissociation triggers structural transformations in Co_3Ag_3 and $CoAg_5$. However, dissociation of H_2 on the silver rich cluster $CoAg_5$ is an endothermic process.

Overall, the binding energies of H_2 (in the molecular adsorption case) and of the two H atoms (in the dissociative adsorption case) to the alloy nanoclusters are higher for the intermediate composition Co_3Ag_3, as compared to the compositions rich in one component, and the activation barrier for dissociation is only 0.042 eV. This is a result which supports the idea that alloying can give a boost in the search for novel nanocatalysts by using the relative atomic composition as a new variable, in addition to cluster size, to optimize the catalyst activity and selectivity for specific reactions.

Data availability

See Supplementary Material for the Cartesian coordinates of the atoms in the Co_nAg_m clusters, bare and with adsorbed hydrogen-

Declaration of competing interest

The authors declare that they have no known competing financial interests or personal relationships that could have appeared to influence the work reported in this paper.

Acknowledgements

Work supported by Ministerio de Ciencia e Innovación of Spain, Grant PID2019-104924RB-I00 funded by MCIN/AEI/10.13039/501100011033, and University of Valladolid (GIR Nanostructure Physics). Estefanía Germán acknowledges a postdoctoral contract with the University of Valladolid. The authors thankfully acknowledge the facilities provided by Centro de Proceso de Datos-Parque Científico (University of Valladolid).

Appendix A. Supplementary data

Supplementary data to this article can be found online at https://doi.org/10.1016/j.ijhydene.2022.04.090.

REFERENCES

[1] Alonso JA. Electronic and atomic structure, and magnetism of transition metal clusters. Chem Rev 2000;100:637–77.
[2] Alonso JA. Structure and properties of atomic nanoclusters. 2nd ed. London: Imperial College Press; 2012.
[3] Hayashi T, Tanaka K, Haruta M. Selective vapor-phase epoxidation of propylene over Au/TiO_2 catalysts in the presence of oxygen and hydrogen. J Catal 1988;178:566–75.
[4] Haruta M, Yamada N, Kobayashi T, Iijima S. Gold catalysts prepared by coprecipitation for low-temperature oxidation of hydrogen and of carbon monoxide. J Catal 1989;115:301–9.
[5] Halder A, Curtiss LA, Fortunelli A, Vajda S. Perspective: size selected clusters for catalysis and electrochemistry. J Chem Phys 2018;148:110901.
[6] Jimenez-Izal, Liu J-Y, Alexandrova AN. Germanium as key dopant to boost the catalytic performance of small platinum clusters for alkane dehydrogenation. J Catal 2019;374:93–100.
[7] Zandkarimi B, Alexandrova AN. Dynamics of subnanometer Pt clusters can break the scaling relationships in catalysis. J Phys Chem Lett 2019;10:460–7.
[8] Gerber IC, Serp Ph. A theory/experience description of support effects in carbon-supported catalysts. Chem Rev 2020;120:1250–349.
[9] Moseler M, Walter M, Yoon B, Landman U, Habibpour V, Harding Ch, Kunz S, Heiz U. Oxidation state and symmetry of magnesia-supported $Pd_{13}O_x$ nanocatalysts influence activation barriers of CO oxidation. J Am Chem Soc 2012;134:7690–9.
[10] Lang SM, Fleischer I, Bernhardt Th M, Barnett RN, Landman U. Low-temperature CO oxidation catalyzed by free palladium clusters: similarities and differences to Pd surfaces and supported particles. ACS Catal 2015;5:2275–89.
[11] Wei Wentao, Lu Yizhong, Chen Wei, Chen Shaowei. One-pot synthesis, photoluminescence, and electrocatalytic properties of subnanometer-sized copper clusters. J Am Chem Soc 2011;133:2060–3.
[12] Lei Y, Mehmood F, Lee S, Greeley J, Lee B, Seifert S, Winans RE, Elam JW, Meyer RJ, Redfern PC, Teschner D, Schlögl R, Pellin MJ, Curtiss LA, Vajda S. Increased silver activity for direct propylene epoxidation via subnanometer size effects. Science 2010;328:224–8.
[13] Molina LM, Lee S, Sell K, Barcaro G, Fortunelli A, Lee B, Seifert S, Winans RE, Elam JW, Pellin MJ, Barke I, von Oeynhausen V, Lei Y, Meyer RJ, Alonso JA, Fraile Rodríguez A, Kleibert A, Giorgio S, Henry CR, Meiwes-Broer K-H, Vajda S. Size-dependent selectivity and activity of silver nanoclusters in the partial oxidation of propylene to propylene oxide and acrolein: a joint experimental and theoretical study. Catal Today 2011;160:116–30.
[14] Henckens MLCM, Driessen PPJ, Worrell E. Metal scarcity and sustainability, analyzing the necessity to reduce the extraction of scarce metals. Resour Conserv Recycl 2014;93:1–8.
[15] Montejano-Carrizales JM, Iñiguez MP, Alonso JA. Embedded-atom method applied to bimetallic clusters: the Cu-Ni and Cu-Pd systems. Phys Rev B 1994;49:16649–58.
[16] Ferrando R, Jellinek J, Johnston RL. Nanoalloys: from theory to applications of alloy clusters and nanoparticles. Chem Rev 2008;108:845–910.
[17] Spadaro MC, Humphrey JJL, Cai R, Martínez L, Haigh SJ, Huttel Y, Spencer SJ, Wain AJ, Palmer R. Electrocatalytic behaviour of PtCu clusters produced by nanoparticle beam deposition. J Phys Chem C 2020;124:23683–9.
[18] Lee JD, Jishkariani D, Zhao Y, Najmr S, Rosen D, Kikkawa JM, Stach EA, Murray Ch B. Tuning the electrocatalytic oxygen reduction reaction activity of Pt–Co nanocrystals by cobalt concentration with atomic-scale understanding. ACS Appl Mater Interfaces 2019;11:26789–97.
[19] Toshima N, Yonezawa T. Bimetallic nanoparticles – novel materials for chemical and physical applications. New J Chem 1998;22:1179–201.
[20] Alexeev OS, Gates BC. Supported bimetallic cluster catalysts. Ind Eng Chem Res 2003;42:1571–87.
[21] Sankar M, Dimitratos N, Miedziak PJ, Wells PP, Kiely CJ, Hutchings GJ. Designing bimetallic catalysts for a green and sustainable future. Chem Soc Rev 2012;41:8099–139.
[22] Shan Shiyao, Petkov V, Prasai B, Wu Jinfang, Joseph P, Skeete Z, Kim Eunjoo, Mott D, Malis O, Luo J, Zhong Chuan-Jian. Catalytic activity of bimetallic catalysts highly sensitive to the atomic composition and phase structure at the nanoscale. Nanoscale 2015;7:18936–48.
[23] Ayodele OB, Cai R, Wang J, Ziouani Y, Liang Z, Spadaro MC, Kovnir K, Arbiol J, Akola J, Palmer RE, Kolen'ko YV. Synergistic computational–experimental discovery of highly

selective PtCu nanocluster catalysts for acetylene semihydrogenation. ACS Catal 2020;10:451–7.
[24] Neukermans S, Janssens E, Chen ZF, Silverans RE, Schleyer PvR, Lievens P. Extremely stable metal-encapsulated $AlPb_{10}^{+}$ and $AlPb_{12}^{+}$ clusters: mass-spectrometric discovery and density functional theory study. Phys Rev Lett 2004;92:163401.
[25] Chen Z, Neukermans S, Wang X, Janssens E, Zhou Z, Silverans RE, King RB, Schleyer PvR, Lievens P. To achieve stable spherical clusters: general principles and experimental confirmations. J Am Chem Soc 2006;128:12829–34.
[26] Bhattacharyya, Nguyen TT, Haeck JD, Hansen K, Lievens P, Janssens E. Mass-selected photodissociation studies of $AlPb_{n}^{+}$ clusters (n = 7–16): evidence for the extraordinary stability of $AlPb_{10}^{+}$ and $AlPb_{12}^{+}$. Phys Rev B 2013;87:054103.
[27] Donís A, López MJ, Alonso JA. Bimetallic Al–Sn clusters: mixing at the nanoscale. Phys Chem Chem Phys 2019;21:22919–29.
[28] Janssens E, Van Hoof T, Veldeman N, Neukermans S, Houb M, Lievens P. Mass spectrometric and modeling investigations of bimetallic silver–cobalt clusters. Int J Mass Spectrom 2006;252:38–46.
[29] Marín P, Alonso JA, Germán E, López MJ. Nanoalloys of metals which do not form bulk alloys: the case of Ag–Co. J Phys Chem A 2020;124:6468–77.
[30] Itaoka K, Saito A, Sasaki K. Public perception on hydrogen infrastructure in Japan: influence of rollout of commercial fuel cell vehicles. Int J Hydrogen Energy 2017;42:7290–6.
[31] Salmeron M. The nature of the catalytic sites for H_2 dissociation. Top Catal 2005;36:55–62.
[32] Auras SV, van Lent R, Bashlakov D, Piñeiros Bastidas JM, Roorda T, Spierenburg R, Juurlink LBF. Scaling platinum-catalyzed hydrogen dissociation on corrugated surfaces. Angew Chem Int Ed 2020;59:20973–9.
[33] Calle-Vallejo F, Martínez JI, García-Lastra JM, Sautet P, Loffreda D. Fast prediction of adsorption properties for platinum nanocatalysts with generalized coordination numbers. Angew Chem Int Ed 2014;53:8316–9.
[34] Cabria I, López MJ, Fraile S, Alonso JA. Adsorption and dissociation of molecular hydrogen on palladium clusters supported on graphene. J Phys Chem C 2012;116:21179–89.
[35] Blanco-Rey M, Juaristi JI, Alducin M, López MJ, Alonso JA. Is spillover relevant for hydrogen adsorption and storage in porous carbons doped with palladium nanoparticles? J Phys Chem C 2016;120:17357–64.
[36] Righi G, Magri R, Selloni A. H_2 dissociation on noble metal single atom catalysts adsorbed on and doped into CeO_2 (111). J Phys Chem C 2019;123:9875–83.
[37] Alducin M, Juaristi JI, Granja-DelRío A, López MJ, Alonso JA. Dynamics of cluster isomerization induced by hydrogen adsorption. J Phys Chem C 2019;123:15236–43.
[38] Ogden JM. Hydrogen: the fuel of the future? Phys Today 2002;55(4):69–75.
[39] Fuel cell handbook. 7th ed. Morgantown: EG&G Technical Services, Inc. US Dept. of Energy; 2004.
[40] Jiao Kui, Jin Xuan, Du Qing, Bao Zhiming, Xie Biao, Wang Bowen, Zhao Yan, Fan Linhao, Wang Huizhi, Hou Zhongjun, Huo Sen, Brandon Nigel P, Yin Yan, Guiver MD. Designing the next generation of proton-exchange membrane fuel cells. Nature 2021;595:361–9.
[41] Cabria I, López MJ, Alonso JA. Hydrogen storage capacities of nanoporous carbon calculated by density functional and Möller-Plesset methods. Phys Rev B 2008;78:075415.
[42] Wang L, Yang RT. New sorbents for hydrogen storage by hydrogen spillover - a review. Energy Environ Sci 2008;1:268–79.
[43] Cabria I, López MJ, Alonso JA. Simulation of the hydrogen storage in nanoporous carbons with different pore shapes. Int J Hydrogen Energy 2011;36:10748–59.
[44] Jena P. Materials for hydrogen storage: past, present, and future. J Phys Chem Lett 2011;2:206211.
[45] Xu W-C, Takahashi K, Matsuo Y, Hattori Y, Kumagai M, Ishiyama S, Kaneko K, Iijima S. Investigation of hydrogen storage capacity of various carbon materials. Int J Hydrogen Energy 2007;32:2504–12.
[46] Yürüm Y, Taralp A, Veziroglu T. Storage of hydrogen in nanostructured carbon materials. Int J Hydrogen Energy 2009;34:3784–98.
[47] Laikhtman A, Michaelson S, Hoffman A, Kim TK, Moon HR, Zak A. Using hydrogen activated by microwave plasma vs. molecular hydrogen for hydrogen storage in tungsten disulfide inorganic nanotubes. Int J Hydrogen Energy 2014;39:9837–41.
[48] Zhang G, Kandlikar SG. A critical review of cooling techniques in proton exchange membrane fuel cell stacks. Int J Hydrogen Energy 2012;37:2412–29.
[49] Antunes RA, Oliveira MCL, Ett G, Ett V. Corrosion of metal bipolar plates for PEM fuel cells: a review. Int J Hydrogen Energy 2010;35:3632–47.
[50] Mizoguchi J, Kanegae T, Takahashi H. Dissociation of H_2 into H^+ in high-dielectric media for fuel-cell applications. Jpn J Appl Phys 2008;47:2262–4.
[51] Conner W, Falconer J. Spillover in heterogeneous catalysis. Chem Rev 1995;95:759–88.
[52] Prins R. Hydrogen spillover. Facts and fiction. Chem Rev 2012;112:2714–38.
[53] Karim W, Spreafico C, Kleibert A, Gobrecht J, VandeVondele J, Ekinci Y, van Bokhoven JA. Catalyst support effects on hydrogen spillover. Nature 2017;541:68–71.
[54] Contescu CI, Brown CM, Liu Y, Bhat VV, Gallego NC. Detection of hydrogen spillover in palladium modified activated carbon fibers during hydrogen adsorption. J Phys Chem C 2009;113:5886–90.
[55] Bhat VV, Contescu CI, Gallego NC, Baker FS. Atypical hydrogen uptake on chemically-activated, ultramicroporous carbon. Carbon 2010;48:1331–40.
[56] Contescu CI, van Benthem K, Li S, Bonifacio CS, Pennycook SJ, Jena P, Gallego NC. Single Pd atoms in activated carbon fibers and their contribution to hydrogen storage. Carbon 2011;49:4050–8.
[57] Lu WJ, Shi DT, Burger A, Collins WE. Comparison of morphology and interfacial composition of Pd ultrathin films on 6H–SiC and 4H–SiC at different annealing temperatures. J Vac Sci Technol 1999;17:1182–90.
[58] Tong Xiaogang, Ma Li, Yin Yuehong, Chen Hongshan. Adsorption and dissociation of molecular hydrogen on Na_3Al_5 and Na_5Al_5. Chem Phys Lett 2020;758:137922.
[59] Guo L. First-principles study of molecular hydrogen adsorption and dissociation on Al_nCr (n = 1–13) clusters. J Phys Chem A 2013;117:3458–66.
[60] Boruah B, Kalita B. Exploring enhanced hydrogen adsorption on Ti doped Al nanoclusters: a DFT study. Chem Phys 2019;518:123–33.
[61] Jia M, Vanbuel J, Ferrari P, Schöllkopf W, Fielicke A, Nguyen MT, Janssens E. Hydrogen adsorption and dissociation on $Al_nRh_2^{+}$ (n = 1 to 9) clusters: steric and coordination effects. J Phys Chem C 2020;124:7624–33.
[62] Charkin OP, Maltsev AP. Density functional theory modeling of reactions of addition of H_2 molecules to magnesium clusters $Mg_{17}M$ doped with atoms M of transition 3d elements. J Phys Chem A 2021;125:2308–15.
[63] Trivedi R, Bandyopadhyay D. Hydrogen storage in small size Mg_nCo clusters: a density functional study. Int J Hydrogen Energy 2015;40:12727–35.

[64] Trivedi R, Bandyopadhyay D. Study of adsorption and dissociation pathway of H_2 molecule on Mg_nRh (n = 1-10) clusters: a first principle investigation. Int J Hydrogen Energy 2016;41:20113–21.
[65] Davis JBA, Horswell SL, Piccolo L, Johnston RL. J Organomet Chem 2015;792:190–3.
[66] Oumellal Y, Matei Ghimbeu C, Martínez de Yuso A, Zlotea C. Hydrogen absorption properties of carbon supported PdNi nanoalloys. Int J Hydrogen Energy 2017;42:1004–11.
[67] Kohn W, Sham LJ. Self-consistent equations including exchange and correlation effects. Phys Rev 1965;140:A1133–8.
[68] Sholl D, Steckel J,A. Density functional theory. A practical introduction. John Wiley & Sons; 2011.
[69] Giannozzi P, Baroni S, Bonini N, Calandra M, Car R, Cavazzoni C, Ceresoli D, Chiarotti GL, Cococcioni M, Dabo I, et al. Quantum espresso: a modular and open-source software project for quantum simulations of materials. J Phys Condens Matter 2009;21:395502.
[70] Kresse G, Joubert D. From ultrasoft pseudopotentials to the projector augmented-wave method. Phys Rev B 1999;59:1758–75.
[71] Blöchl E. Projector augmented-wave method. Phys Rev B 1994;50:17953–79.
[72] Monkhorst H, Pack J. Special points for Brillouin-zone integration. Phys Rev B 1976;13:5188–92.
[73] Perdew JP, Burke K, Ernzerhof M. Generalized gradient approximation made simple. Phys Rev Lett 1996;77:3865–8.
[74] Grimme S, Antony J, Ehrlich S, Krieg H. A consistent and accurate ab initio parametrization of density functional dispersion correction (DFT-D) for the 94 elements H-Pu. J Chem Phys 2010;132:154104.
[75] Vanbuel J, Germán E, Libeert G, Veys K, Moens J, Alonso JA, López MJ, Janssens E. Reactivity of cobalt-fullerene complexes towards deuterium. ChemPhysChem 2020;21:1012–8.
[76] Germán E, Alonso JA, Janssens E, López MJ. $C_{60}Co_n$ complexes as hydrogen adsorbing materials. Int J Hydrogen Energy 2021;46:20594–606.
[77] Farkas B, Terranova U, Leeuw NH. The mechanism underlying the functionalization of cobalt nanoparticles by carboxylic acids: a first-principles computational study. J Mater Chem B 2021;9:4915. 4028.
[78] López MJ, Marcos PA, Alonso JA. Structural and dynamical properties of Cu-Au bimetallic clusters. J Chem Phys 1996;104:1056–66.
[79] Jellinek J, Krissinel EB. Alloys clusters: structural clases, mixing, and phase changes. In: Jellinek J, editor. Theory of atomic and molecular clusters with a glimpse at experiments. Berlin: Springer-Verlag; 1999. p. 277–308.
[80] García-Díez K, Fernández-Fernández J, Alonso JA, López MJ. Theoretical study of the adsorption of hydrogen on cobalt clusters. Phys Chem Chem Phys 2018;20:21163–76.
[81] Kleis J, Greeley J, Romero NA, Morozov VA, Falsig H, Larsen AH, Lu J, Mortensen JJ, Dulak M, Thygesen KS, Norskov JK, Jacobsen KW. Finite size effects in chemical bonding: from small clusters to solids. Catal Lett 2011;141:1067–71.
[82] Bader RFW. Atoms in molecules. Acc Chem Res 1985;18:9–15.
[83] Bader RFW. Atoms in molecules-A quantum theory. Oxford University Press; 1990.
[84] Tang W, Sanville E, Henkelman G. A grid-based Bader analysis algorithm without lattice bias. J Phys Condens Matter 2009;21:084204.
[85] Henkelman G, Uberuaga BP, Jónsson H. A climbing image nudged elastic band method for finding saddle points and minimum energy paths. J Chem Phys 2000;113:9901–4.
[86] Granja-DelRío A, Alonso JA, López MJ. Steric and chemical effects on the hydrogen adsorption and dissociation on free and graphene-supported palladium clusters. Comput Theoret Chem 2017;1107:23–9.
[87] Gálvez-González LE, Alonso JA, Paz-Borbón LO, Posada-Amarillas A. H_2 adsorption on $Cu_{4-x}M_x$ (M = Au, Pt; x = 0-4) clusters: similarities and differences as predicted by Density Functional Theory. J Phys Chem C 2019;123:30768–80.
[88] Gómez Herranz A, Germán E, Alonso JA, López MJ. Interaction of hydrogen with Palladium-Copper nanoalloys. Theoret Chem Accounts 2021;140:35.